

Article

Assessment of *Warionia saharea* Essential Oil as a Green Corrosion Inhibitor for Mild Steel in HCl: Experimental and Computational Studies

Abdeslam Ansari ¹, Youssef Youssefi ¹, Mohamed Tanghourte ¹, Nazih Ouassou ¹, Nazih Asoufar ¹, Mohamed Znini ¹, Hassane Lgaz ^{2,*}, El Houssine Mabrouk ¹, Mohamed Azrou ¹, Han-Seung Lee ^{3,*} and Belkheir Hammouti ⁴

¹ Laboratory of Materials Engineering for the Environment & Natural Resources, Faculty of Science and Technology, University Moulay Ismail of Meknes, BP 509, Errachidia 52003, Morocco;

ansdesa2@yahoo.fr (A.A.); y.youssefi@edu.umi.ac.ma (Y.Y.); m.tanghourte@edu.umi.ac.ma (M.T.); n.ouassou@edu.umi.ac.ma (N.O.); n.asoufar@edu.umi.ac.ma (N.A.); m.znini@umi.ac.ma (M.Z.); mabrouk.elhoussine@gmail.com (E.H.M.); m.azrou@fste.umi.ac.ma (M.A.)

² Innovative Durable Building and Infrastructure Research Center, Center for Creative Convergence Education, Hanyang University ERICA, 55 Hanyangdaehak-ro, Sangrok-gu, Ansan-si 15588, Gyeonggi-do, Republic of Korea

³ Department of Architectural Engineering, Hanyang University ERICA, 55 Hanyangdaehak-ro, Sangrok-gu, Ansan-si 15588, Gyeonggi-do, Republic of Korea

⁴ Euromed University of Fes, UEMF, Fes 30000, Morocco; hammoutib@gmail.com

* Correspondence: hlgaz@hanyang.ac.kr (H.L.); ercleehs@hanyang.ac.kr (H.-S.L.)



Citation: Ansari, A.; Youssefi, Y.; Tanghourte, M.; Ouassou, N.; Asoufar, N.; Znini, M.; Lgaz, H.; Mabrouk, E.H.; Azrou, M.; Lee, H.-S.; et al. Assessment of *Warionia saharea* Essential Oil as a Green Corrosion Inhibitor for Mild Steel in HCl: Experimental and Computational Studies. *Coatings* **2024**, *14*, 1164. <https://doi.org/10.3390/coatings14091164>

Academic Editors: Patricia Jovičević-Klug, Matic Jovičević-Klug and László Tóth

Received: 4 July 2024

Revised: 7 August 2024

Accepted: 3 September 2024

Published: 9 September 2024



Copyright: © 2024 by the authors. Licensee MDPI, Basel, Switzerland. This article is an open access article distributed under the terms and conditions of the Creative Commons Attribution (CC BY) license (<https://creativecommons.org/licenses/by/4.0/>).

Abstract: The objective of this research work is the study of the inhibitory effect of *Warionia saharea* essential oil (WSEO) on the corrosion of mild steel (MS) in molar HCl solution, employing both experimental and theoretical methods. This inhibitory effect (IE) has been evaluated by using a combination of weight loss measurements (LW) and various electrochemical methods, such as open circuit potential (OCP), potentiodynamic polarization (PDP) and electrochemical impedance spectroscopy (EIS) experiments. The LW results indicated that IE increased with inhibitor concentration, reaching 83.34% at 3.00 g/L. The PDP analysis suggested that WSEO functions as a mixed inhibitor, while in the EIS results the R_{ct} values increased with inhibitor concentration to reach $165.8 \Omega \text{ cm}^2$ at 2.00 g/L, suggesting a defensive film formation by WSEO molecules over the metallic surface. The thermodynamic study demonstrated that the WSEO molecules adsorption on the MS surface followed a Langmuir isotherm, involving mixed physical and chemical (physicochemical) adsorption on the MS surface. Theoretical methods, including density functional theory (DFT) and molecular dynamics (MD) simulations, were employed to elucidate the inhibition mechanisms of the three main components of WSEO. The quantum chemical analysis, using density functional theory (DFT) and molecular dynamics (MD) simulations, showed a low ΔE_{gap} value of 6.30 eV and a low adsorption energy (E_{ads}) value on an Fe (110) substrate of -258 Kcal/mol for (E)-Nerolidol, indicating the significant contribution of this molecule to the overall corrosion inhibition effect of WSEO. The scanning electron microscope (SEM) analysis verified the presence of a protective film formed by the inhibitor on the MS surface. This study highlights the potential of WSEO as a sustainable and green corrosion inhibitor in acidic environments.

Keywords: *Warionia saharea*; mild steel; corrosion inhibition; molecular dynamics

1. Introduction

The problems of deterioration of steel-based metal structures now occupy a fundamental place in the industry, particularly during descaling and acid pickling [1,2]. In this regard, effective means must be developed to control and/or prevent corrosion of these industrial parts. Currently, the exploration of components typically derived from natural

sources, such as essential oils (EOs) extracted from various aromatic plants, as ecofriendly corrosion inhibitors, has proven to be an effective and promising way to reduce corrosion rates while minimizing economic losses and environmental and health impacts, because these alternatives are biodegradable, easy to extract and non-toxic [3,4]. This type of corrosion-inhibiting material has been proved effective in mitigating corrosion along with other inhibiting options such as carbon quantum dots [5]. For instance, the inhibitive effect of *Schinus mole* EO against the corrosion of carbon steel in 1.0 M HCl solution was reported and the corrosion inhibition performance was as high as 70% at 25 °C at 2 g/L [6]. The inhibitive action of Vietnam orange peel EO for MS in 1.0 M HCl solution has been investigated, and the maximum effectiveness (about 90%) was obtained at 3–4 g/L [6]. The EO of *Aaronsohnia pubescens* subsp. *pubescens* was reported as a green corrosion inhibitor for MS in 1.0 M HCl with a maximum performance of 89.88% at 3 g/L [7]. The inhibitory performance of these EOs results from their wide range of active centers such as functional groups (C=O, CO-O, O-H) and fragments composed of π electrons from double bonds and the aromatic cycle, which is capable of adsorbing on metal surfaces [3–8].

Environmentally friendly alternatives can have minimal health, environmental and safety risks and reasonably high protection efficiency at relatively low concentrations. The use of several environmentally friendly alternatives, including nanomaterials such as carbon dots (CDs) and their derivatives as well as plant extracts such as essential oils, has been extensively investigated as environmentally friendly alternatives to toxic corrosion inhibitors. However, in terms of preparation, essential oils are obtained via a simple and easy-to-use apparatus that only requires water as a solvent. For nanomaterials, their preparation requires nanomaterials, sometimes solvents, energy and time (i.e., multiple steps). In terms of application, essential oils have some disadvantages such as solubility in corrosive environments, supply (low yield) and mixing complexity. In addition, nanomaterials such as carbon dots have the following advantages: productivity, single-product synthesis, solubility (water as a solvent for preparation) and efficiency.

Furthermore, competitive interactions and synergistic effects between various molecules can coexist around the active regions of the metal surface, making it difficult to determine precisely which components present in the mixture can have a significant impact on corrosion suppression. However, it can be assumed that the main components are possible candidates that contribute to corrosion inhibition [7,9]. To confirm this hypothesis, it is desirable to study experimentally and individually the inhibitory power of each major component in corrosive environments, but this process is long and laborious, and sometimes the mechanism of inhibition remains unexplained. In this context, computational methods, such as density functional theory (DFT) and molecular dynamics (MD) simulations, have been developed as complementary approaches to explain complex “inhibitor/surface” interactions occurring in the corrosion process [10].

In an earlier investigation conducted in our laboratory, *Warionia saharea* essential oil (WSEO) was evaluated for its efficacy as an eco-friendly corrosion inhibitor for mild steel (MS) in a 0.5 M H₂SO₄ solution. The study revealed that WSEO achieved a maximum inhibition efficiency of 74% at a concentration of 3 g/L [11]. Building upon these findings, the present study focuses on assessing the corrosion inhibitory properties of WSEO on mild steel in a more aggressive 1 M HCl environment. We accomplished this by utilizing weight loss (WL) measurements in conjunction with electrochemical methods, specifically potentiodynamic polarization (PDP) and electrochemical impedance spectroscopy (EIS). These methods allowed for a comprehensive evaluation of WSEO's performance as a corrosion inhibitor under different conditions and provided deeper insights into its mechanism of action in acidic media.

The structure–activity relationship between the electronic/molecular properties of the main components and the WSEO efficiency was demonstrated by quantum chemical calculations using density functional theory (DFT). Molecular dynamics simulations were also carried out to describe the adsorption process of these molecules on the Fe (110) surface.

In parallel, a characterization of the surface of the steel was carried out using a scanning electron microscope (SEM).

2. Materials and Methods

2.1. Materials Preparation

Corrosion tests were carried out on MS samples having the following chemical composition (wt.%): P (0.09%), S (0.05%), Si (0.01%), Al (0.05%), Mn (0.21%) and the remainder iron. The corrosive medium was 1 M HCl prepared from a commercial HCl (37%) solution in distilled water.

The inhibitor used in this study was the WSEO extracted and characterized as described previously in our research [11]. It was obtained by hydrodistillation for 3 h using a Clevenger type apparatus with an average yield of 1.2%. Thirty-nine compounds, representing 93.2% of the total oil, were identified by gas chromatography (GC) and gas chromatography/mass spectroscopy (GC/MS). Figure 1 shows the names and structures of the three major components of WSEO: β -Eudesmol (34.9%), (E)-Nerolidol (23.0%) and Linalool (15.2%).

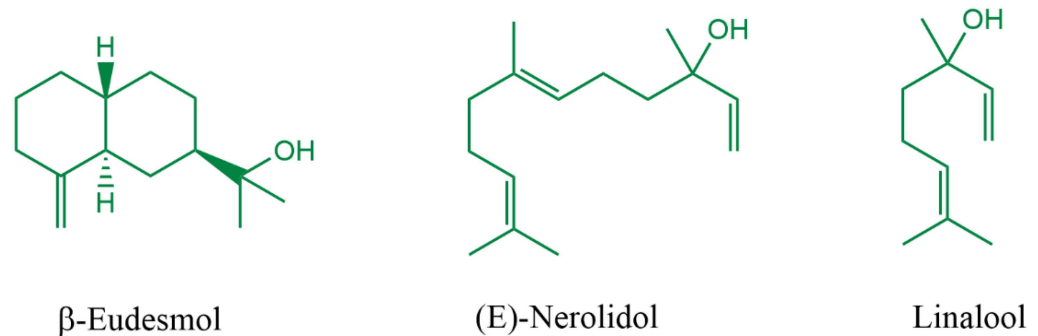


Figure 1. Chemical structures of the major components of WSEO.

2.2. Corrosion Tests

The inhibitory effects of *Warionia saharea* essential oil (WSEO) against MS corrosion in 1 M HCl were assessed using chemical and electrochemical methods, following the methodology previously established in our research [9]. To evaluate the inhibitor's protective efficacy, various concentrations of WSEO, ranging from 0.25 to 3.00 g/L, were tested. The essential oil was initially dissolved in pure ethanol to ensure uniform dispersion and effective interaction with the corrosive medium.

For the WL measurements, the inhibition efficiency (IE_{WL}) (%) was calculated based on Equation (1):

$$IE_{WL} \% = \frac{W_{\text{corr}} - W_{\text{corr(inh)}}}{W_{\text{corr}}} \times 100 \quad (1)$$

where W_{corr} and $W_{\text{corr(inh)}}$ are the values of the corrosion rate of MS in uninhibited and inhibited solutions, respectively.

For the electrochemical tests, firstly, the working electrode's open circuit potential (OCP) was tested for a period of 1800 s to achieve the stable corrosion potential (E_{corr}) value.

The inhibition efficiency (IE_{PDP} %) in PDP assay was calculated by the following Equation (2):

$$IE_{\text{PDP}} (\%) = \left(\frac{i_{\text{corr}} - i_{\text{corr, inh}}}{i_{\text{corr}}} \right) \times 100 \quad (2)$$

where i_{corr} and $i_{\text{corr, inh}}$ represent the corrosion current densities without and in the presence of the inhibitor, respectively.

In the case of the EIS test, the inhibitory efficiency (IE_{EIS}) (%) can be calculated using the following Equation (3):

$$IE_{EIS} (\%) = \left(\frac{R'_{ct} - R_{ct}}{R'_{ct}} \right) \times 100 \quad (3)$$

where R_{ct} and R'_{ct} are the charge-transfer resistance values without and with the inhibitor, respectively.

2.3. Scanning Electron Microscope (SEM) Analysis

SEM is generally employed to analyze microstructural and morphological changes in metal surfaces caused by corrosion. Specimens for characterization experiments were MS plates (3 mm × 3 mm × 1 mm). Three MS coupons were prepared in the laboratory by being rubbed with numerous abrasive papers ranging from 180 to 2000, then soaked in acetone as a degreasing solution, washed with double-distilled water, dried between two filter papers, resulting in a mirror finish, and stored in a desiccator.

Afterwards, two coupons were immersed in acidic solutions, both in the absence and presence of 2.00 g/L of the investigated inhibitor, at a constant temperature of 298 K for a duration of 24 h. The surface morphology of the metal was analyzed using scanning electron microscopy (JSM-IT500HR instrument (Tokyo, Japan)), operating at an accelerating voltage of 30 kV and with a magnification of about 20 μm.

2.4. Computational Studies

2.4.1. DFT Investigations

To correlate the obtained inhibition efficiency of WSEO with the molecular structure of its main compounds, some chemical reactivity indicators were calculated. Full geometry optimization was carried out using DFT calculations with the B3LYP level of theory and 6-311++ G (d,p) basis set [12]. Global quantum descriptors, such as E_{HOMO} , E_{LUMO} , and $\Delta E = E_{LUMO} - E_{HOMO}$ (Equation (4)), electronegativity (χ Equation (5)), overall hardness (η Equation (6)) and electron transfer proportion (ΔN Equation (7)), were calculated [13,14].

$$\Delta E_{gap} = E_{LUMO} - E_{HOMO} \quad (4)$$

$$\chi = \frac{E_{LUMO} - E_{HOMO}}{2} \quad (5)$$

$$\eta = \frac{E_{HOMO} - E_{LUMO}}{2} \quad (6)$$

$$\Delta N = \frac{\varnothing - \chi_{inh}}{2(\eta_{Fe} + \eta_{inh})} \quad (7)$$

In this context, \varnothing , which has a value of 4.82, represents the magnitude of the work function. The hardness of iron (Fe) is denoted as $\eta_{Fe} = 0$ eV/mol. The terms χ_{inh} and η_{inh} correspond to the electronegativity and hardness of the inhibitor, respectively. These parameters are essential for understanding the electronic interactions between the inhibitor molecules and the metal surface [15].

2.4.2. Molecular Dynamics Simulation

MD simulations were conducted to describe the adsorption of the three main components on metal surfaces. The simulation was conducted using the Forcite module in the Materials Studio 2020 software. The interactions within the studied system were modeled using a simulation box with dimensions of 24.82 Å × 24.82 Å × 34 Å. The energy surface was minimized using molecular mechanics, then the preliminary surface of 10 Å increased, and its periodicity was reformed by constructing a supercell. At last, the vacuum slab with a 26 Å thickness was constructed on the iron Fe (110) surface. The study was carried out in the solution, which is a mixture of 1 inhibitor molecule, 300 molecules of

H₂O, 20 molecules of H₃O⁺, and Cl⁻ [16,17]. After the system achieves equilibrium, (E_{ads}), the energy of adsorption of the primary chemicals was computed. This was done using Equation (8) [18]:

$$E_{\text{ads}} = (E_{\text{solution}} + E_{\text{total}}) - (E_{\text{inhibitor+solution}} + E_{\text{surface+solution}}) \quad (8)$$

The mean square displacement (MSD) method is used to analyze the interactions between inhibitor molecules and corrosive species and find whether they affect the mobility and movement of particles inside the inhibitor film. In such a way, an amorphous cell module embedded in the Materials Studio 2020 program was used to generate the inhibitor film which held 50 parts (β -Eudesmol, (E)-Nerolidol, Linalool) monomer, 1 part Cl⁻ and 1 part H₃O⁺ with the supercell size (23.450 Å × 23.45 Å × 23.45 Å) [19,20]. After the initial optimization, the MD equilibrium process was carried out, for 300 ps (1 fs time step) in a canonical ensemble (NVT) at 298 K. A Berendsen thermostat managed the system's temperature. All simulations used the COMPASS II force field [21,22].

3. Results and Discussion

3.1. WL Measurements

Table 1 provides a summary of the values of the corrosion rate (W_{corr}), inhibition efficiency (IE_{WL} %) and surface coverage ($\theta = IE_{\text{WL}}/100$) obtained by WL measurements in 1 M HCl with and without different doses of WSEO after 24 h of immersion at 25 °C.

Table 1. WL measurements of MS after 6 h immersion in blank and inhibited solutions by WSEO at 25 °C.

C_{WSEO} (g/L)	0.00	0.25	0.50	1.00	2.00	3.00
W_{corr} (mg·cm ⁻² h ⁻¹)	0.381	0.098	0.090	0.076	0.065	0.063
IE_{WL} (%)	-	74.15	76.36	79.96	82.93	83.34
Surface coverage (θ)	-	0.7415	0.7636	0.7996	0.8293	0.8334

The obtained results revealed that WSEO inhibits the MS's corrosion in a dose-dependent manner. With the addition of the inhibitor, W_{corr} is delayed and IE_{WL} (%) is significantly increased. Thus, IE_{WL} (%) goes from a value of 74.15% at 0.25 g/L to optimal and maximum values of 82.93 and 83.34% at 2.00 and 3.00 g/L, respectively. This characteristic explains the role of chemical composition of WSEO that is mainly electron-rich in inhibiting the corrosion [7,9]. In a previous study, the maximum value of IE_{WL} (%) of WSEO for MS corrosion in 0.5 H₂SO₄ solution was 74% at 3 g/L [11]. As a comparison, it can be noticed that the IE_{WL} (%) values of WSEO are higher in 1 M HCl compared to those in 0.5 H₂SO₄ throughout the concentration range tested, suggesting that the nature of the anions could influence the adsorption of the tested essential oil in acid solutions. This is consistent with previous studies that have demonstrated that the adsorption capacity of chloride ions (Cl⁻) on the surface is more powerful than that of sulfate ions (SO₄²⁻) [23,24]. Finally, the nature of the anions can affect the adsorption of the tested inhibitor in acidic solutions.

3.2. OCP Measurements

Figure 2 shows the evolution of the OCP during immersion of an MS in a 1 M HCl solution without and with different concentrations of WSEO at 298 K.

The results illustrated in Figure 2 clearly show that the potential (OCP) of the MS immersed in the 1 M HCl acid solution without and with inhibitor shows an increase to reach a quasi-stationary state at about 1800 s of immersion time, which indicates that the steel electrode/solution interface has reached a stable condition. Furthermore, with the increase in the concentration of inhibitors, a shift of OCP towards more positive values is noted. These variations can be justified by the formation of a layer on the surface of the electrode blocking the reactions that occur on the MS, such as the oxidation of iron and the reduction of hydrogen ions from hydrochloric acid [25].

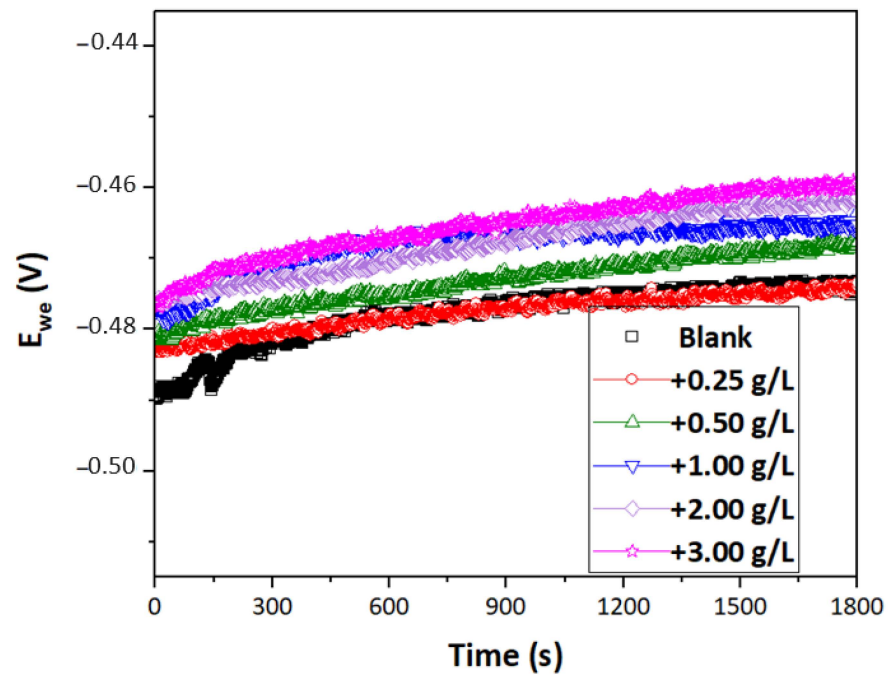


Figure 2. OCP–time curves for MS in 1 M HCl without and with various concentrations of WSEO.

3.3. Potentiodynamic Polarization Curves

PDP curves for MS in a 1 M HCl solution, both without and with various concentrations of WSEO, were measured at 25 °C, and the results are illustrated in Figure 3. The key polarization parameters, including corrosion current density (i_{corr}), corrosion potential (E_{corr}), cathodic Tafel slope (β_c), anodic Tafel slope (β_a) and inhibition efficiency ($IE_{PDP}\%$), are detailed in Table 2. These parameters provide a comprehensive overview of the inhibitory performance and electrochemical behavior of WSEO in the acidic medium.

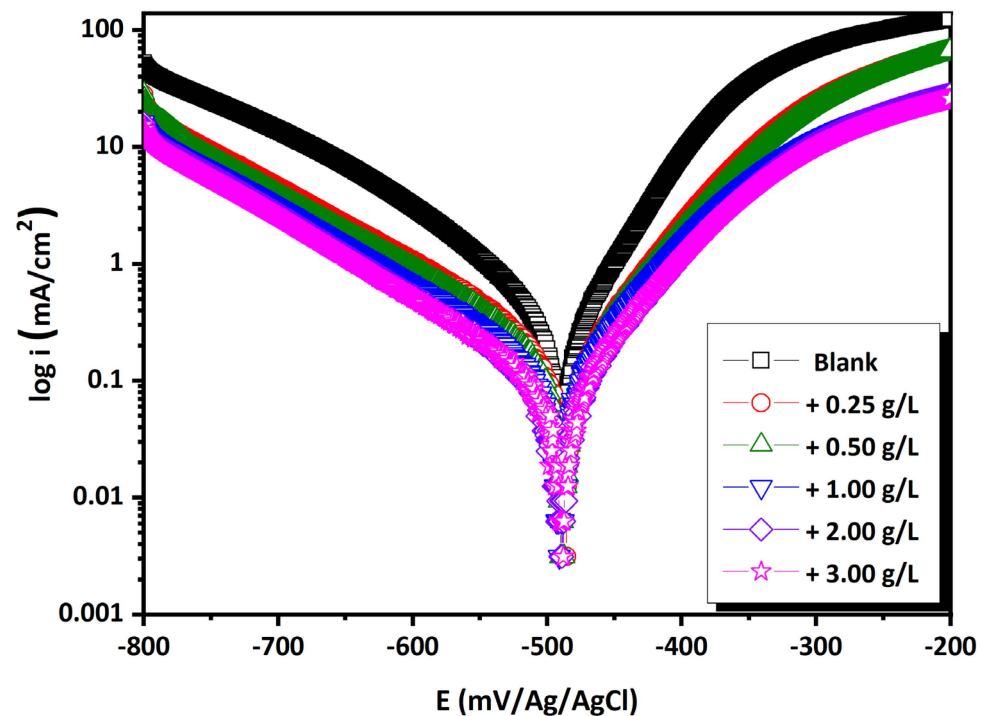


Figure 3. PDP curves of mild steel (MS) in 1.0 M HCl with and without varying concentrations of *Warionia saharea* essential oil (WSEO) at 25 °C.

Table 2. PDP parameters for mild steel (MS) in 1 M HCl with and without different concentrations of *Warionia saharea* essential oil (WSEO) at 25 °C.

C_{WSEO} (g/L)	$-E_{corr}$ (mV/SCE)	i_{corr} ($\mu\text{A cm}^{-2}$)	$-\beta_c$ (mV dec $^{-1}$)	β_a (mV dec $^{-1}$)	IE_{PDP} (%)	θ
0.00	490	578.0	147.7	74.8	-	-
0.25	490	152.5	157.3	56.7	73.62	0.7362
0.50	490	130.6	149.8	53.6	77.40	0.7740
1.00	480	101.6	144.1	53.2	82.42	0.8242
2.00	480	92.4	140.8	49.9	84.01	0.8401
3.00	480	91.8	138.9	48.6	84.11	0.8411

Figure 3 demonstrates that the addition of WSEO significantly reduces both anodic and cathodic current densities. This reduction indicates a strong adsorption tendency of the oil on the MS surface, effectively delaying both anodic and cathodic reactions. These observations suggest that WSEO functions as a mixed-type inhibitor, providing comprehensive protection by impeding both the anodic and cathodic processes involved in corrosion [7,8]. The analysis of Table 2 clearly indicates that the IE_{PDP} (%) gradually increases with the addition of WSEO to the 1 M HCl solution until reaching its optimal value of 84.01% at 2.00 g/L. Further, the addition of the inhibitor changed the cathodic (β_c) and anodic (β_a) Tafel slopes in the inhibited system. This suggests that during the inhibition process, the inhibition mainly controls the cathodic and anodic reactions [7]. In addition, a slight shift of values of E_{corr} (below 85 mV) was detected, especially at high inhibitor concentrations, indicating the mixed character of the inhibitor and thus confirming the reduction of hydrogen evolution and metal oxidation [25].

3.4. EIS Measurements

Nyquist diagrams for MS corrosion in 1 M HCl solution and in the presence of different concentrations of the WSEO at 25 °C are shown in Figure 4a. The obtained EIS spectra were analyzed by fitting to the equivalent circuit illustrated in Figure 4b using EC-LAB V10.32 software, and the results are presented in Table 3.

Table 3. EIS values for MS in 1 M HCl with varying WSEO concentrations at 25 °C.

C_{WSEO} (g/L)	R_{ct} ($\Omega \text{ cm}^2$)	C_{dl} ($\mu\text{F cm}^2$)	CPE		IE_{EIS} (%)	θ	χ^2 (10^{-3})
			Q ($\Omega^{-1}\text{S}^n\text{cm}^{-2}$)	n			
0.00	21.71	73.37	314.51	0.877	-	-	2.25
0.25	69.1	52.52	219.23	0.865	68.58	0.6858	3.52
0.50	80.2	48.08	118.04	0.866	72.93	0.7293	5.40
1.00	134.8	42.78	96.70	0.864	83.90	0.8390	3.25
2.00	165.8	38.42	82.21	0.836	86.91	0.8691	5.25
3.00	166.1	37.64	82.11	0.834	86.92	0.8792	5.41

The Nyquist plots depicted in Figure 4a display a single capacitive loop for each test, suggesting that charge transfer is the primary mechanism controlling the corrosion processes in 1 M HCl [26]. This finding aligns with the single time constant observed in the Bode plots shown in Figure 4c,d. However, these capacitive loops are not ideal semicircles, which can be attributed to the dispersion effect commonly caused by the surface roughness and heterogeneity of the solid surfaces [27].

Moreover, as the concentration of the inhibitor increases, the width of the Nyquist plots also expands, indicating enhanced adherence of the natural substance to the mild steel (MS) surface. This increased width reflects the inhibitor's improved effectiveness in forming a protective barrier, thereby mitigating the corrosion process. The findings under-

score the potent adsorption capabilities of the inhibitor, reinforcing its role in providing substantial protection against corrosion in acidic environments.

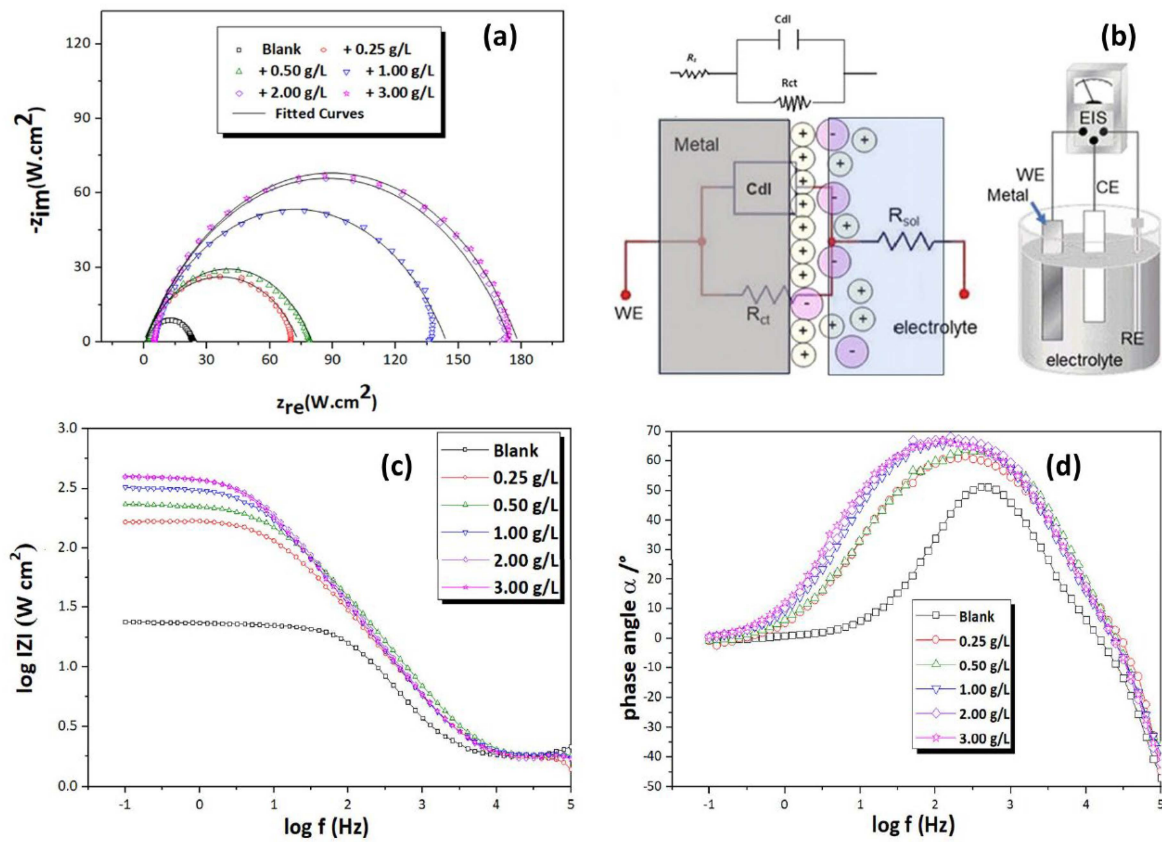


Figure 4. Nyquist diagrams (a), equivalent circuit (b) and Bode plots (c,d) of MS in 1 M HCl without and with the addition of various concentrations of WSEO at 25 °C.

Figure 4b shows the equivalent electrochemical circuit used to simulate the MS/acidic solution interface, where R_s is the solution resistance, R_{ct} is the charge transfer resistance and CPE is the constant-phase element to replace the double-layer capacitor (C_{dl}). The CPE element is employed to consider the heterogeneous surface of the working electrode and is defined by Equation (9) [2]:

$$Z_{CPE} = Q^{-1} \cdot ((i \cdot \omega))^{-n} \tag{9}$$

where $i^2 = -1$, imaginary root; Q , CPE constant; ω , angular frequency (in rads^{-1}); n , deviation indicator which is a measure of surface inhomogeneity and its value lies between 0 and 1. $n = 1$ represents the ideal capacitor, $n = 0.5$ represents Warburg impedance, $n = -1$ represents inductance and $n = 0$ represents a resistor [27].

The fitting degree between the experimental data and the simulated results obtained by the proposed equivalent circuit was evaluated by the chi-square (χ^2) parameter (fit goodness).

The values of the double-layer capacitance (C_{dl}) were determined using the following formula of Equation (10) [3]:

$$C_{dl} = (Q \cdot R_{ct}^{1-n})^{1/n} \tag{10}$$

Based on Table 3, it can be seen that R_{ct} values rise with rising WSEO concentration. The highest R_{ct} value ($166.1 \Omega \text{ cm}^2$) has been obtained at 3.00 g/L, indicating the adsorption of the inhibitor and the development of a protective layer at the MS/solution interface that restricts the accessibility of Cl^- ions to the metal surface [28]. Alternatively, the C_{dl} value decreases with the addition of EO; it changes from $73.37 \mu\text{F} \cdot \text{cm}^2$ for the blank medium only to $37.64 \mu\text{F} \cdot \text{cm}^2$ for 3.00 g/L of WSEO. This diminution of C_{dl} values with the addition of

the molecule can be explained by the rises in the dielectric constant and/or an increasing thickness of the electrical double layer.

Consequently, the IE_{EIS} values (%) show that the highest inhibitory performance is observed at the optimum concentration (2.00 g/L) and reach a maximum 87%. This result suggests that WSEO acts as a good adsorption inhibitor at the solution/metal interface forming a film or complex repelling corrosive species from the MS surface [14]. This behavior is in good agreement with that noticed from the WL and PDP results. Furthermore, the capacitance values of the double layer are also reduced to the maximum in the presence of the studied inhibitor compared to the uninhibited solution. The decrease in C_{dl} with increasing inhibitor concentration can be attributed to a decrease in the local dielectric constant and an increase in the thickness of the electrical double layer [28].

Moreover, the data in Table 3 clearly show that the values of the parameter χ^2 are very low on the order of 10^{-3} , which explains the agreement of the experimental impedance spectra with the proposed equivalent electrical circuit. In addition, it is noted that the surface heterogeneity parameter n changes with the addition of the inhibitor, indicating the surface modification when the WSEO is added [28]. In addition, the values of n remained relatively constant at around 0.8 (approaching unity), suggesting that the CPE is getting closer to the ideal capacitor behavior.

On the other hand, in a comparative study of the EO extracted from *W. saharea*, we note, according to Table 4, that the WSEO presents an excellent inhibitory performance in comparison with the other extracts of different and even low concentrations, which implies the importance of WSEO in the industrial sector.

Table 4. Comparison of WSEO inhibition efficiencies with those of other essential oils.

EO Inhibitor	Medium and Substrate	Concentration	IE (%)	Ref
<i>Schinus mole</i>	CS in 1 M HCl	2.00 g/L	70%	[6]
<i>Vietnam orange peel</i>	MS in 1 M HCl	4.00 g/L	about 90%	[7]
<i>A. pubescens</i> subsp. <i>pubescens</i>	MS in 1 M HCl	3.00 g/L	89.88%	[8]
<i>Myrtle</i>	Copper in 3% NaCl	10.00 g/L	91.88%	[27]
<i>Rosemary</i>			92.54%	
<i>Asteriscus graveolens</i>	MS in 0.5 M H ₂ SO ₄	3.00 g/L	82.89%	[28]
<i>Warionia saharea</i>	MS in 0.5 M H ₂ SO ₄	3.00 g/L	74%	[11]
<i>Warionia saharea</i>	MS in 1 M HCl	2.00 g/L	84%–87%	In this work

3.5. Adsorption Study

Adsorption isotherms are used to provide basic information about the nature of the interaction that takes place between the inhibitor and the metal surface. Indeed, to better describe the adsorption mode of WSEO molecules, attempts have been made to adjust the inhibitor concentration (C_{WSEO}) and the surface coverage values (θ) to certain adsorption isotherms such as the Langmuir isotherms, El-Awady, Freundlich and Temkin.

The linear equations (Equations (S1)–(S4)) of the studied isotherms are shown in Table S1 (Supplementary Materials) and their corresponding plots are represented in Figure 5. Depending on the model used, assumed differences can be taken into account such as the nature of the metallic surface and the interactions between the adsorbed molecules, as well as the structure of the layers formed by adsorbed species [29]. The correlation coefficient between surface coverage (θ) and the inhibitor concentration (C_{WSEO}) in the corroding solution were compared.

The equilibrium constant of the adsorption process K_{ads} is related to the Gibbs standard free energy of adsorption (ΔG°_{ads}) by the following relationship (Equation (11)) [6].

$$\Delta G^\circ_{ads} = -RT \ln (55.5 K^\circ_{ads}) \quad (11)$$

where R is the universal gas constant, T is the thermodynamic temperature and 55.5 is the concentration of water in solution expressed in M (i.e., ~1000 g/L). Table 5 summarizes the estimated parameters from the studied isotherm graphs.

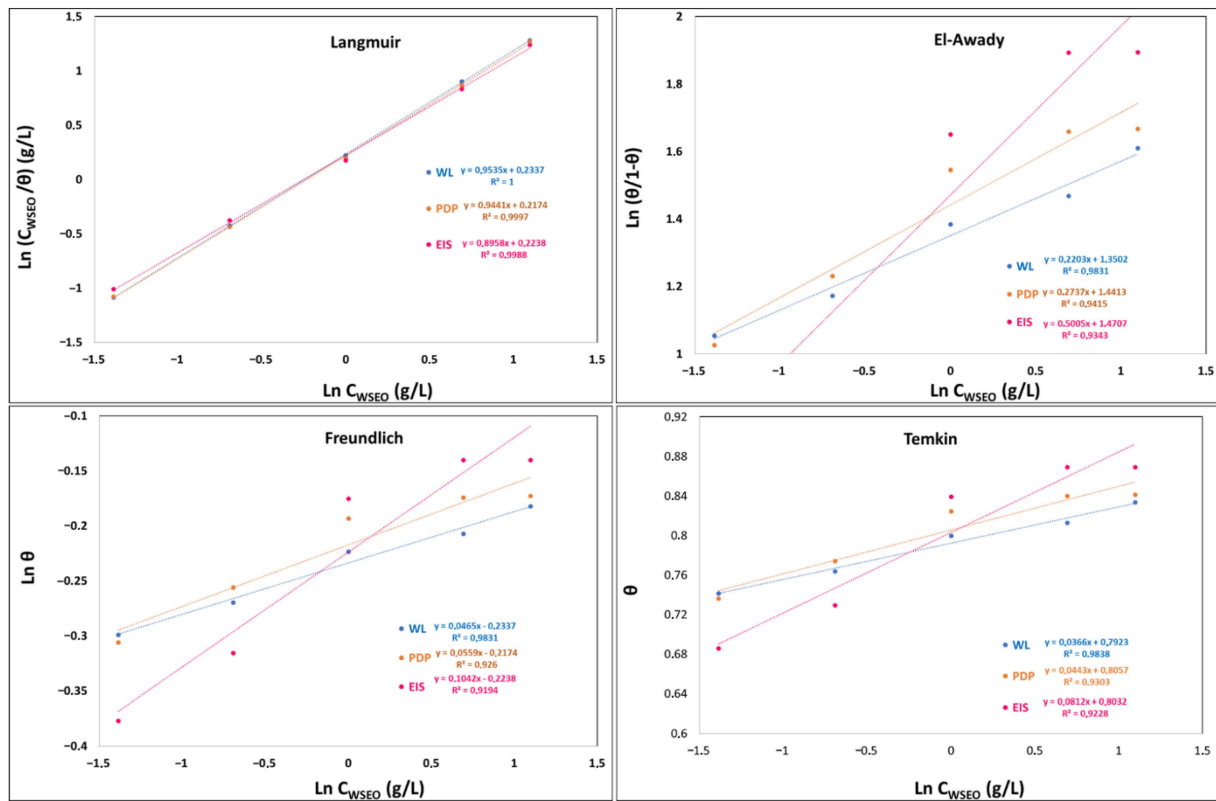


Figure 5. Isotherm models tested for MS in 1 M HCl in presence of WSEO using WL, PDP and EIS data at 25 °C.

Table 5. Thermodynamic finding for MS in 1 M HCl in the presence of WSEO at 25 °C.

Adsorption	Method	R ²	K _{ads} (L/g)	Isotherm Property	ΔG ^o _{ads} (KJ·mol ⁻¹)
Langmuir	WL	1	0.79	R _L = 0.39	−16.55
	PDP	0.9997	0.81	R _L = 0.38	−16.60
	EIS	0.9998	0.80	R _L = 0.38	−16.58
El-Awady	WL	0.9831	459.43	1/y = 4.54	−32.33
	PDP	0.9415	192.48	1/y = 3.65	−30.18
	EIS	0.9343	18.72	1/y = 2.00	−24.40
Freundlich	WL	0.9831	0.79	z = 0.047	−16.55
	PDP	0.926	0.80	z = 0.056	−16.58
	EIS	0.9194	0.80	z = 0.104	−16.58
Temkin	WL	0.9838	250 × 10 ⁶	a = −13.66	−65.08
	PDP	0.9303	78.6 × 10 ⁶	a = −11.28	−62.22
	EIS	0.9228	19.7 × 10 ³	A = −6.15	−41.65

Examination of the plots presented in Figure 5 and the values listed in Table 5 revealed that the correlation coefficients (R²) for all adsorption isotherms range from 0.91 to 1. It is clear that the corresponding plots of the Langmuir isotherm are straight lines with the correlation coefficients (R²) close to unity (R² > 0.999) and that the values of the separation factor R_L are between 0 and 1, which confirms that the Langmuir isotherm model describes the appropriate adsorption of WSEO molecules on the MS surface in the acidic medium. However, the slope values are less than unity, suggesting that the real adsorption of the

WSEO did not strictly respect this isotherm. There may have been multilayer adsorption of inhibitor molecules or lateral interactions between the adsorbed species and the MS surface. According to the El-Awady adsorption parameter, the inverse of “*y*” obtained is between 2 and 4, suggesting that the WSEO molecule replaces up to four water molecules during the inhibition process schematized as follows (Equation (12)) [29,30].



Since the value of the adsorption parameter “*z*” in the Freundlich isotherm is less than 1, it is likely that the inhibitor studied will readily bind to the metal surface. Regarding the Temkin adsorbent isotherm, the values of the attractive parameter (*a*) are negative in all cases, showing that the lateral interaction is repulsive in the adsorption layer [31].

Generally, $\Delta G^\circ_{\text{ads}}$ values lower than $-20 \text{ KJ}\cdot\text{mol}^{-1}$ are linked to physical adsorption (physisorption), while $\Delta G^\circ_{\text{ads}}$ values negatively greater than $40 \text{ KJ}\cdot\text{mol}^{-1}$ correspond to chemical adsorption (chemisorption). However, a physicochemical adsorption process (mixed adsorption) was observed when the $\Delta G^\circ_{\text{ads}}$ displayed intermediate values between $-20 \text{ KJ}\cdot\text{mol}^{-1}$ and $-40 \text{ KJ}\cdot\text{mol}^{-1}$ [32]. In our study, $\Delta G^\circ_{\text{ads}}$ of the inhibitor ranged between -16 and $-65 \text{ KJ}\cdot\text{mol}^{-1}$, indicating a physicochemical adsorption process onto the metal surface. Additionally, negative values of $\Delta G^\circ_{\text{ads}}$ indicate spontaneous adsorption of molecules onto the MS surface, as well as strong interaction between active sites of molecules and the metal surface [4].

3.6. SEM Analysis

To gain deeper insights into the adsorption of WSEO molecules on the MS surface, we conducted a surface morphology analysis using scanning electron microscopy (SEM). Figure 6 presents the SEM images of mild steel (MS) immersed in 1 M HCl, both without and with 2.00 g/L of WSEO, after a 24 h exposure period.

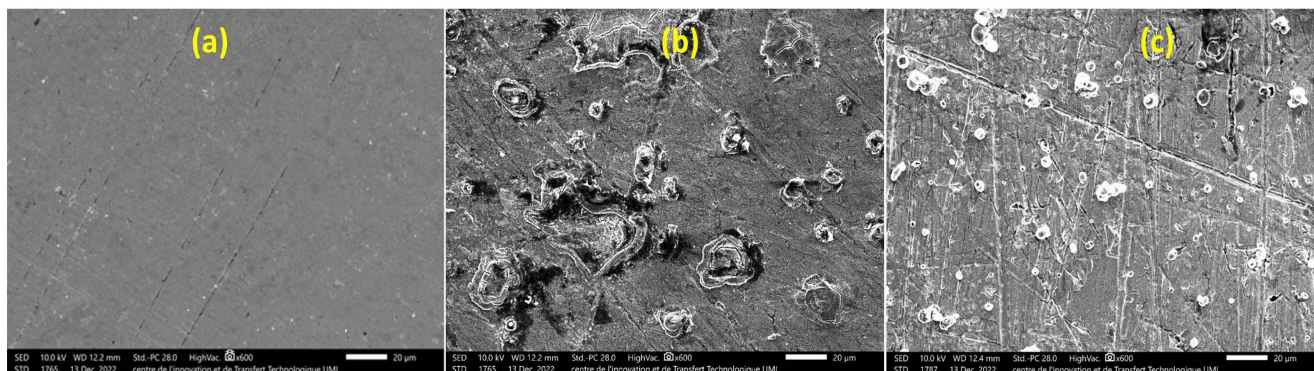


Figure 6. SEM morphology of MS surface (a) before immersion, (b) after 24 h immersion in blank solution and (c) after 24 h immersion in inhibited solution.

The morphology of MS after polishing and before exposure to the corrosive solution shows that the metal surface is clearly visible and has a characteristic associated with polishing scratches Figure 6a. After immersion in the corrosive solution without inhibitor, the SEM micrograph Figure 6b shows that the surface of the MS is seriously damaged due to the aggressive attack of the acid solution. However, by adding 2.00 g/L of WSEO, the surface morphology of the MS appears smoother and less corroded (Figure 6c). This behavior can be explained by the formation of a protective film adsorbed by WSEO molecules on the surface of the steel, which leads to a reduction in the corrosion process [33].

3.7. Theoretical Studies

3.7.1. DFT Calculations

Usually, EOs include various phytochemical components [5]. Because of this complexity, it is challenging to identify the components of an EO that could significantly contribute to preventing corrosion, but it can be assumed that phytochemicals with the highest percentages are responsible for EO performance [7,9]. In this regard, a DFT/B3LYP with 6-311++ G (d,p) basis set study was performed to correlate the inhibitive effect of the entire WSEO and the electronic properties of its major constituents (β -Eudesmol (34.9%), (E)-Nerolidol (23.0%) and Linalool (15.2%).

Figure 7 illustrates optimized structures and LUMO-HOMO plots of β -Eudesmol, (E)-Nerolidol, and Linalool. Table 6 lists some global quantum chemical descriptors.

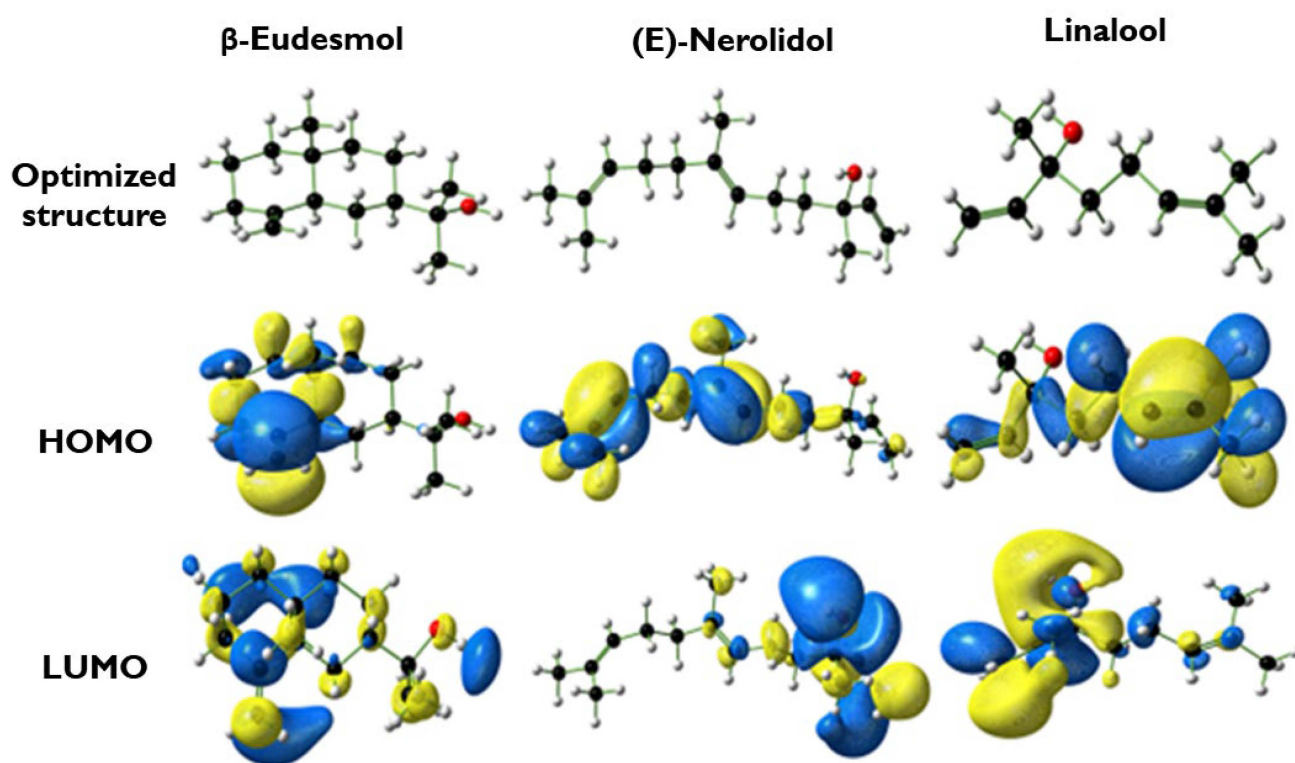


Figure 7. The HOMO-LUMO iso-surfaces and optimized geometry for β -Eudesmol, (E)-Nerolidol and Linalool that have been evaluated by the DFT/B3LYP with 6-311++ G (d,p) basis set.

Table 6. Calculated theoretical parameters for the major components of WSEO obtained from the DFT/B3LYP with 6-311++ G (d,p) basis set.

Molecule	E_{HOMO} (eV)	E_{LUMO} (eV)	ΔE_{gap} (eV)	ΔN	η
β -Eudesmol	−6.35	0.86	7.21	0.29	3.61
(E)-Nerolidol	−6.01	0.29	6.30	0.31	3.15
Linalool	−6.36	0.56	6.92	0.28	3.46

HOMO plots illustrate the regions of a molecule where electron donation is likely to occur, with a higher E_{HOMO} value signifying a greater propensity for the molecule to transfer electrons to the metal's unoccupied orbitals. Conversely, the density of the LUMO indicates the areas where the molecule can receive electrons, and a lower E_{LUMO} value denotes a stronger ability of the molecule to accept electrons from the metal surface [34]. Consequently, high E_{HOMO} values and low E_{LUMO} values favor the ability of the inhibitor to bind to the metal surface; thus, a low value of $\Delta E_{\text{gap}} = E_{\text{LUMO}} - E_{\text{HOMO}}$ increases the molecular reactivity and is expected to improve the inhibitory efficiency [35]. Figure 6 reveals that

the HOMO and LUMO distributions for β -Eudesmol are similar, which were mostly situated around the methylcyclohexane motif. For (E)-Nerolidol, the HOMO density is mostly on the total molecule and is strongly spread around the (-C=C-) fraction, while the LUMO density is distributed over the atoms of the α , β -unsaturated hydroxyl group. The HOMO and LUMO orbitals for Linalool are similar and more intense along with the terminal double bond.

According to Table 6, (E)-Nerolidol has the highest E_{HOMO} and the lowest E_{LUMO} compared with β -Eudesmol and Linalool, which suggests that (E)-Nerolidol has the strong donor–acceptor properties. Likewise, the values of ΔE_{gap} and η follow the same theoretical order following (E)-Nerolidol < Linalool < β -Eudesmol, which shows that (E)-Nerolidol is more reactive than the β -Eudesmol. In addition, the ΔN value of (E)-Nerolidol is slightly higher than that of other molecules, which confirms the strong electron exchange of this molecule to and/or from the iron surface [36]. Based on the obtained findings, (E)-Nerolidol is expected to contribute to the corrosion inhibition of WSEO to a large extent, followed by Linalool and then β -Eudesmol.

3.7.2. MD Simulations

The optimized molecule–Fe (110) adsorption systems simulated by MD in the aqueous phase are shown in Figure 8. Correspondingly, the resulting adsorption energies calculated with MD simulation are listed in Table 7.

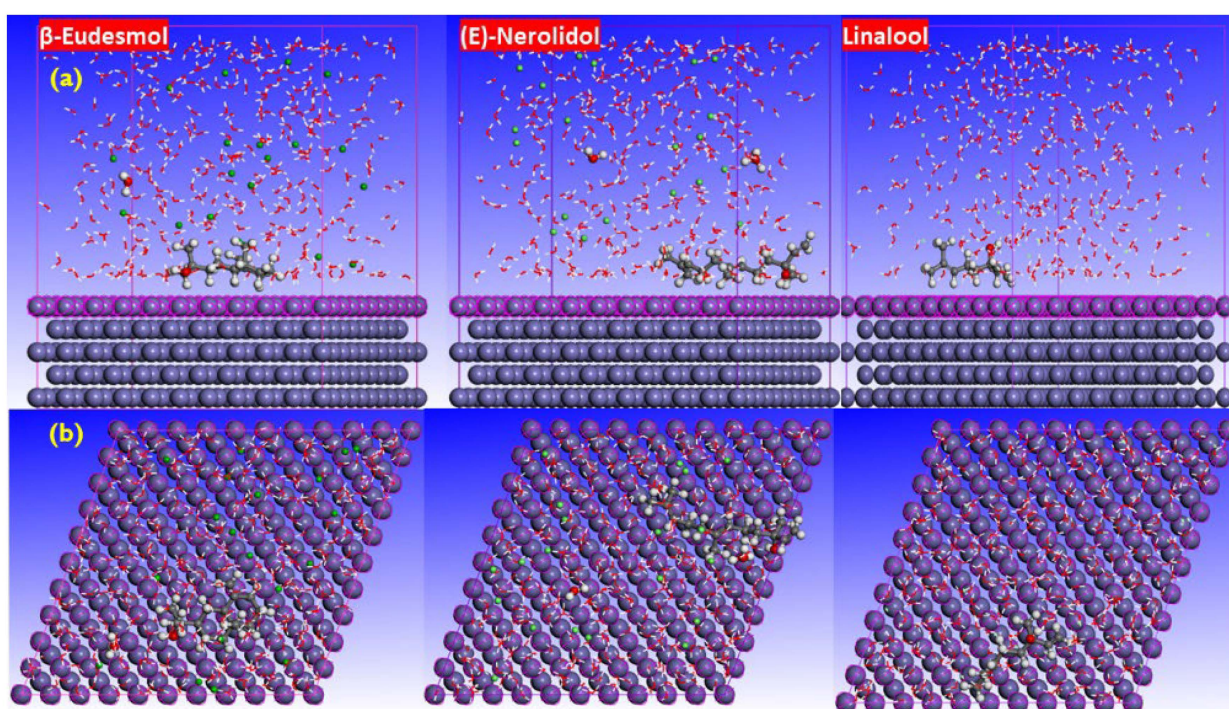


Figure 8. Top (a) and side (b) view of the most equilibrium adsorption configurations of the selected WSEO components on an Fe (110) surface obtained by MD simulations in the aqueous phase.

Table 7. The adsorption energies for the adsorption of the three main compounds of WSEO on the Fe (110) surface obtained by MD simulations (all in kcal/mol).

Molecule	E_{ads}
β -Eudesmol	−215.18
(E)-Nerolidol	−258.15
Linalool	−140.60

From Figure 8, it can be seen that the selected components of the WSEO are optimally adsorbed in a planar direction parallel to the surface of the Fe (110), thus maximizing the coverage of this surface thanks to the protective film created by the inhibitors causing the isolation of water molecules and other corrosive particles from the metal surface.

Moreover, the negative value of the adsorption energy indicates the exothermic and spontaneity of the adsorption process. Also, its high values show a stable and robust adsorption of the inhibitors on the Fe (110) surface, suggesting the rigidity of the interaction of inhibitors on the metal surface, thereby increasing their inhibition efficiency [37].

Table 7 indicates that the values of adsorption for selected molecules are negatives and obey the following order: (E)-Nerolidol > β -Eudesmol > Linalool.

According to Table 7, (E)-Nerolidol exhibits the highest adsorption energy, indicating its stronger affinity to adhere to the Fe surface forming a more stable protective layer against MS corrosion. Therefore, (E)-Nerolidol is the best candidate molecule to contribute substantially to the global corrosion inhibition effect of WSEO.

3.7.3. MSD Analysis

The MSD calculation was carried out in order to evaluate the anticorrosive performance of β -Eudesmol, (E)-Nerolidol and Linalool, by preventing the movement of H_3O^+ and Cl^- present in the corrosive solution. This model is based on the description of the migration rate of a corrosive species in inhibitor films by calculation of their diffusion coefficient (D_{ion}). Generally, the lower the value of the D_{ion} of corrosive species, the lower their migration, and thus the protective capacity of the inhibitor film will be higher [38]. Each supercell includes one cation of H_3O^+ , one anion of Cl^- , and 30 molecules of the EO's main component. The diffusion coefficients of H_3O^+ : $D_{\text{ion}}(\text{H}_3\text{O}^+)$ and Cl^- : $D_{\text{ion}}(\text{Cl}^-)$ resulting from the MSD curves can be determined by Einstein's equation (Equations (13) and (14)) [39,40]:

$$\text{MSD}(t) = \frac{1}{N} \sum_{i=1}^N |R_i(t) - R_i(0)|^2 \quad (13)$$

$$D = \frac{1}{6} \lim_{t \rightarrow \infty} \frac{d\text{MSD}(t)}{dt} \quad (14)$$

where N reflects the number of diffusive atoms, while $R_i(0)$ and $R_i(t)$ translate the positions of corrosive ions at the origin time (0) and a later time (t), respectively.

A low value of D_{ion} means that corrosive species move poorly in the solution, thus preventing the electrochemical corrosion process. Conversely, a high value of D_{ion} suggests that the inhibitor film is weak [41]. Figure 9 displays MSD vs. time curves and the diffusion behaviors of $D_{\text{ion}}(\text{H}_3\text{O}^+)$ and $D_{\text{ion}}(\text{Cl}^-)$ in the supercell containing β -Eudesmol, (E)-Nerolidol and Linalool. In addition, the diffusion of corrosive species occurs via migration between free sites or cavities inside the inhibiting film on the metal surface. One method to examine the factors influencing the diffusion of corrosive species is through the calculation of fractional free volume (FFV). FFV is computed by Equation (15):

$$\text{FFV}(\%) = \frac{V_f}{V_f + V_{\text{oc}}} \times 100 \quad (15)$$

where V_f is the free volume and V_{oc} is the volume occupied by the inhibitor film on the metal surface.

Typically, a high FFV value means that there are free cavities on the inhibition film in which corrosive species move easily from one cavity to another, resulting in a high diffusion coefficient and low efficiency of the inhibitor. Conversely, a low FFV value is associated with a low diffusion coefficient and high corrosion inhibition efficiency [41]. Figure 9 shows the molecular distribution used to calculate the V_f and V_{oc} volumes for systems built with a Connolly area. The calculated D_{ion} and the FFV values of both corrosive species in various inhibitor films are listed in Table 8.

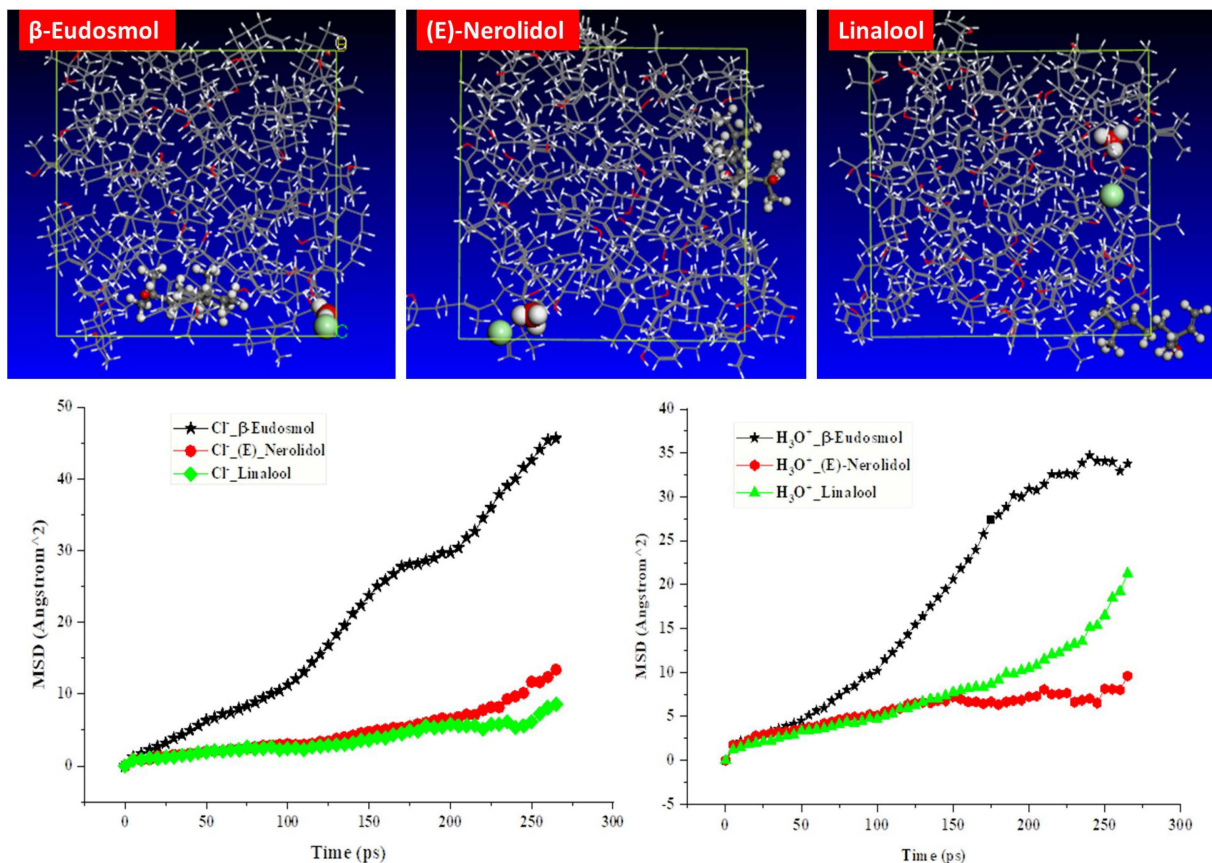


Figure 9. MSD vs. time curves and the diffusion behaviors of corrosive species (H_3O^+ and Cl^- ions) in three condensed inhibitor films at 25 °C.

Table 8. Calculated values of FFV and self-diffusion coefficient of the three molecules.

Molecule	$D_{\text{ion}}(\text{H}_3\text{O}^+)$ ($\text{m}^2 \text{s}^{-1}$)	$D_{\text{ion}}(\text{Cl}^-)$ ($\text{m}^2 \text{s}^{-1}$)	FFV (%)
(E)-Nerolidol	1.926×10^{-3}	1.062×10^{-2}	6.50
Linalool	1.57×10^{-2}	5.114×10^{-3}	6.94
β -Eudesmol	2.144×10^{-2}	3.153×10^{-2}	13.00

From Figure 9, the movement curve of corrosive species in β -Eudesmol is the most typical. It shifts by approximately 35 and 45 Å for H_3O^+ and Cl^- , respectively. However, in the case of (E)-Nerolidol and Linalool, the Cl^- shift curves are relatively smooth and weak (around 10 Å) while the H_3O^+ shift curves are characterized by a sharp jump in the case of Linalool (around 23 Å) at the end of the observation period. Therefore, based on the data in Table 8, we can classify the D_{ion} of H_3O^+ in all the inhibitor films examined as follows: $D_{\text{ion}}(\text{E})\text{-Nerolidol} < D_{\text{ion}}(\text{Linalool}) < D_{\text{ion}}(\beta\text{-Eudesmol})$. This order is in good accordance with the descriptors order reported by DFT calculations.

In Figure 10, we can see that the protective films formed by (E)-Nerolidol and Linalool are denser in the supercell; that is, the metal surface would be more covered than in the case of β -Eudesmol. In addition, from the FFV values (%), the sequence follows the same order as that of D_{ion} : (E)-Nerolidol < Linalool < -Eudesmol. This indicates that FFV decreases with molecular chain structure and length. It is well known that linear structures are more flexible than cyclic structures that are difficult to bend. Indeed, the increase in the linear chain strengthens the inhibition performance of (E)-Nerolidol ($\text{C}_{15}\text{H}_{26}\text{O}$) compared to Linalool ($\text{C}_{10}\text{H}_{18}\text{O}$). However, the bicyclic nature of ($\text{C}_{15}\text{H}_{26}\text{O}$) reduces its adsorption on the metal surface due to its rigidity. Obviously, the addition of these molecules to the solution limits the migration of corrosive species. Finally, the obtained findings confirm

those discussed previously that (E)-Nerolidol may exhibit the highest reactivity among the three phytochemicals.

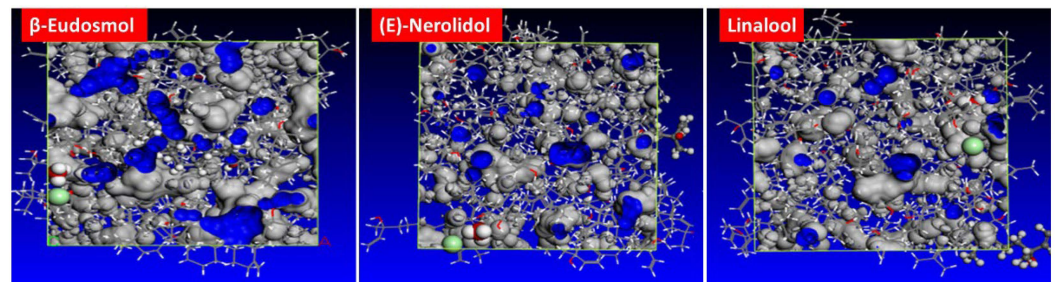


Figure 10. FFV of Cl^- and H_3O^+ in the four condensed inhibitor films at 25 °C.

3.8. Corrosion Inhibition Mechanism of WSEO

The first step in the suppression of the corrosion of metal is often the adsorption of inhibitors at the metal/solution interface. Such a mechanism might be sensitive to the chemical structure of the inhibitor and the metal's surface charge. As a result, the inhibitive activity of WSEO entails the adsorption of its active phytochemical components on the MS surface, particularly its main components namely β -Eudesmol (34.9%), (E)-Nerolidol (23.0%) and Linalool (15.2%). These compounds contain π -electrons of double bonds ($\text{C}=\text{C}$) and atomic oxygen in functional groups ($\text{O}-\text{H}$) that meet the normal adsorption centers. Moreover, extract organic components exist as neutral molecules and/or in the protonated form in the aqueous acid solution. Charged molecules (cations) can be absorbed by opposing charges via direct electrostatic interactions among the negatively charged molecules and the positively charged metal surface. Adsorbing may also be caused by no direct interaction between the protonated form and the chloride ions (Cl^-), primarily adsorbed on the MS surface charged positively (a physical mechanism). The neutral form can adsorb onto metal surfaces via a "donor-acceptor" interaction. This occurs between the non-bonded electron pairs of oxygen atoms and the π -electrons of double bonds, interacting with the "d" orbitals of the mild steel (MS) surface (a chemical mechanism) [4]. In this present study, E-Nerolidol was found to be the best candidate molecule that could significantly contribute to the overall corrosion inhibition effect of EOTL. Figure 11 illustrates the simplified scheme of the adsorption mechanism of E-Nerolidol on the C-steel surface in the 1.00 M HCl medium.

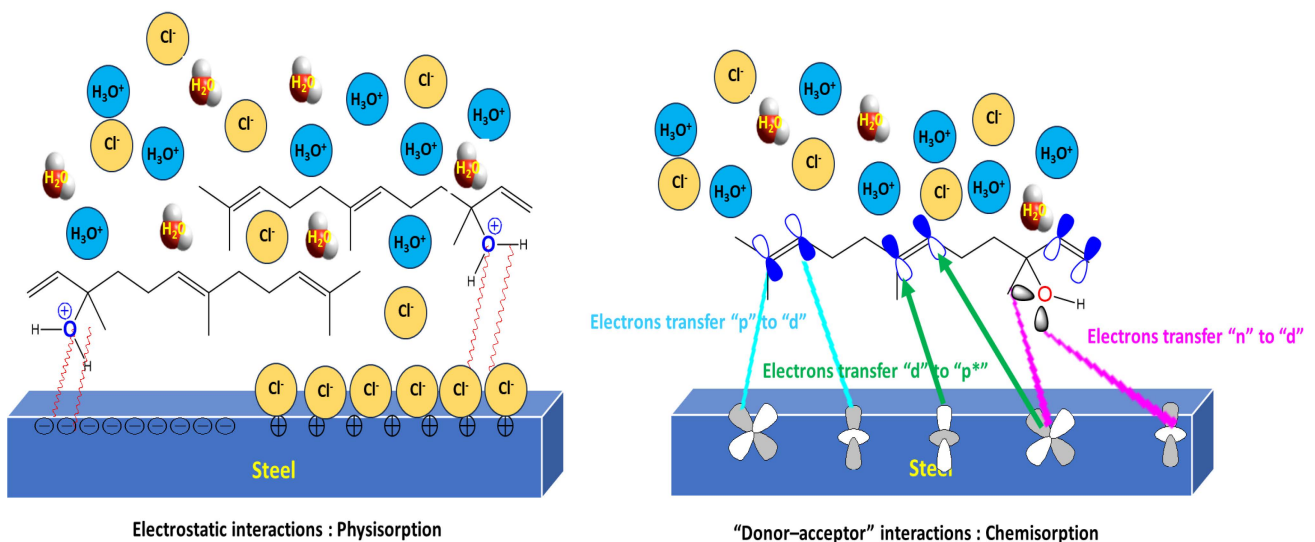


Figure 11. Simplified schema of the adsorption mechanism of (E)-Nerolidol molecules on the MS surface.

4. Conclusions

In this investigation, the inhibition ability of WSEO for MS corrosion in 1 M HCl medium was explored experimentally using weight loss (WL) measurement, electrochemical assays and SEM analysis, as well as theoretically using quantum DFT calculations and MC simulations. The key findings from these experiments are summarized as follows:

1. WSEO has been found to provide a satisfactory IE% of 86% at 2.00 g/L and 298 K, which suggests that it can be used as a good green corrosion inhibitor for MS in 1 M HCl medium.
2. The PDP study demonstrated that the examined inhibitor exerts a mixed inhibition effect and with increasing WSEO concentrations, the i_{corr} values dropped dramatically from 578.0 $\mu\text{A cm}^{-2}$ in a blank solution to 92.4 $\mu\text{A cm}^{-2}$ in the presence of 2.00 g/L, indicating significant corrosion inhibition potential.
3. Based on the EIS data, R_{ct} values rise with rising WSEO concentration reaching the optimal value of 165.8 $\Omega \text{ cm}^2$ at 2.00 g/L, indicating the adsorption of inhibitor and the development of a protective layer at the MS/solution interface.
4. The thermodynamic study revealed that the adsorption of WSEO on the MS surface aligns with the Langmuir isotherm model involving both chemical and physical adsorption.
5. DFT calculations provided a detailed explanation of the relationship between the inhibitory efficacy of WSEO and the electronic properties of its main constituents.
6. Monte Carlo (MC) simulations indicated that the primary compounds preferentially adsorb onto the Fe (110) surface in a flat, parallel orientation.
7. The MSD calculations reveal that the main component of the studied inhibitor creates a barrier film on the MS surface and limits the migration of corrosive species. SEM analysis confirms the existence of an inhibitor protective film on the MS steel surface.
8. The computational results also revealed that (E)-Nerolidol may play an important role in the overall inhibitory action of WSEO in 1 M HCl.

Supplementary Materials: The following supporting information can be downloaded at: <https://www.mdpi.com/article/10.3390/coatings14091164/s1>, Table S1. Linear equations and adsorption isotherms of the studied isotherms of MS in 1 M HCl for WSEO.

Author Contributions: A.A.: Conceptualization, Experiments, Formal Analysis, Resources, Data Curation and Writing the Manuscript; Y.Y., M.T., N.O. and N.A.: Conceptualization, Software, Investigation; E.H.M.: Methodology and Data Curation; M.A.: Validation, Software and Formal Analysis; M.Z.: Methodology, Visualization, Writing the Manuscript, Supervision and Review; H.-S.L. and H.L.: Conceptualization, Visualization, Investigation, Formal Analysis and Writing—Review and Editing; B.H.: Visualization, Supervision and Review. All authors have read and agreed to the published version of the manuscript.

Funding: This work was supported by the National Research Foundation of Korea (NRF), with a grant funded by the Korean government (MSIT) (No. NRF-2018R1A5A1025137).

Institutional Review Board Statement: Not applicable.

Informed Consent Statement: Not applicable.

Data Availability Statement: The data cannot be shared at this time as the data also form part of an ongoing study.

Conflicts of Interest: The authors declare no conflicts of interest.

References

1. Lavanya, D.; Priya, F.V.; Vijaya, D. Green Approach to Corrosion Inhibition of Mild Steel in Hydrochloric Acid by 1-[Morpholin-4-yl (thiophen-2-yl) methyl] thiourea. *J. Fail. Anal. Prev.* **2020**, *20*, 494–502. [[CrossRef](#)]
2. Obot, I.; Meroufel, A.; Onyechu, I.B.; Alenazi, A.; Sorour, A.A. Corrosion inhibitors for acid cleaning of desalination heat exchangers: Progress, challenges and future perspectives. *J. Mol. Liq.* **2019**, *296*, 111760. [[CrossRef](#)]

3. Mzioud, K.; Habsaoui, A.; Ouakki, M.; Galai, M.; El Fartah, S.; Ebn Touhami, M. Inhibition of copper corrosion by the essential oil of *Allium sativum* in 0.5 M H₂SO₄ solutions. *SN Appl. Sci.* **2020**, *2*, 1611. [CrossRef]
4. Znini, M. Application of Essential Oils as green corrosion inhibitors for metals and alloys in different aggressive mediums. *Arab. J. Med. Aromat. Plants* **2019**, *5*, 1–34.
5. Sultana, N.; Hossain, S.; Mohammed, M.E.; Irfan, M.; Haq, B.; Faruque, M.; Razzak, S.; Hossain, M. Experimental study and parameters optimization of microalgae based heavy metals removal process using a hybrid response surface methodology-crow search algorithm. *Sci. Rep.* **2020**, *10*, 15068. [CrossRef]
6. Mellak, N.; Ghali, N.; Messaoudi, N.; Benhelima, A.; Ferhat, M.; Addou, A. Study of corrosion inhibition properties of *Schinus molle* essential oil on carbon steel in HCl. *Mater. Corros.* **2021**, *72*, 1270–1278. [CrossRef]
7. Manssouri, M.; Znini, M.; El Ouadi, Y.; Ansari, A.; Costa, J.; Majidi, L. Essential Oil of *Aaronsohnia Pubescens* Subsp. *Pubescens* as Novel Eco-Friendly Inhibitor for Mild Steel in 1.0 M HCl. *Anal. Bioanal. Electrochem.* **2020**, *12*, 841–856.
8. Bui, H.T.; Dang, T.-D.; Le, H.T.; Hoang, T.T. Comparative study on corrosion inhibition of vietnam orange peel essential oil with urotropine and insight of corrosion inhibition mechanism for mild steel in hydrochloric solution. *J. Electrochem. Sci. Technol.* **2019**, *10*, 69–81.
9. Znini, M.; Ansari, A.; Costa, J.; Senhaji, O.; Paolini, J.; Majidi, L. Experimental, quantum chemical and molecular dynamic simulations studies on the corrosion inhibition of c38 steel in 1M HCl by *Anethum graveolens* essential oil. *Anal. Bioanal. Electrochem.* **2019**, *11*, 1426–1451.
10. Saha, S.K.; Murmu, M.; Murmu, N.C.; Obot, I.; Banerjee, P. Molecular level insights for the corrosion inhibition effectiveness of three amine derivatives on the carbon steel surface in the adverse medium: A combined density functional theory and molecular dynamics simulation study. *Surf. Interfaces* **2018**, *10*, 65–73. [CrossRef]
11. Znini, M.; Majidi, L.; Laghchimi, A.; Paolini, J.; Hammouti, B.; Costa, J.; Bouyanzer, A.; Al-Deyab, S. Chemical composition and anticorrosive activity of Warionia saharea essential oil against the corrosion of mild steel in 0.5 M H₂SO₄. *Int. J. Electrochem. Sci.* **2011**, *6*, 5940–5955. [CrossRef]
12. Frisch, M. Gaussian. 2009. Available online: <http://www.gaussian.com/> (accessed on 21 July 2023).
13. Umar, B.A.; Uzairu, A. In-silico approach to understand the inhibition of corrosion by some potent triazole derivatives of pyrimidine for steel. *SN Appl. Sci.* **2019**, *1*, 1413. [CrossRef]
14. El Ibrahimy, B.; Jmiai, A.; El Mouaden, K.; Baddouh, A.; El Issami, S.; Bazzi, L.; Hilali, M. Effect of solution's pH and molecular structure of three linear α -amino acids on the corrosion of tin in salt solution: A combined experimental and theoretical approach. *J. Mol. Struct.* **2019**, *1196*, 105–118. [CrossRef]
15. Murmu, M.; Saha, S.K.; Murmu, N.C.; Banerjee, P. Effect of stereochemical conformation into the corrosion inhibitive behaviour of double azomethine based Schiff bases on mild steel surface in 1 mol L⁻¹ HCl medium: An experimental, density functional theory and molecular dynamics simulation study. *Corros. Sci.* **2019**, *146*, 134–151. [CrossRef]
16. Errahmany, N.; Rbaa, M.; Abousalem, A.S.; Tazouti, A.; Galai, M.; Touhami, M.E.; Lakhrissi, B.; Touir, R. Experimental, DFT calculations and MC simulations concept of novel quinazolinone derivatives as corrosion inhibitor for mild steel in 1.0 M HCl medium. *J. Mol. Liq.* **2020**, *312*, 113413. [CrossRef]
17. Haldhar, R.; Kim, S.-C.; Prasad, D.; Bedair, M.; Bahadur, I.; Kaya, S.; Dagdag, O.; Guo, L. Papaver somniferum as an efficient corrosion inhibitor for iron alloy in acidic condition: DFT, MC simulation, LCMS and electrochemical studies. *J. Mol. Struct.* **2021**, *1242*, 130822. [CrossRef]
18. Ouakki, M.; Galai, M.; Aribou, Z.; Benzekri, Z.; Dahmani, K.; Ech-chihbi, E.; Abousalem, A.S.; Boukhris, S.; Cherkaoui, M. Detailed experimental and computational explorations of pyran derivatives as corrosion inhibitors for mild steel in 1.0 M HCl: Electrochemical/surface studies, DFT modeling, and MC simulation. *J. Mol. Struct.* **2022**, *1261*, 132784. [CrossRef]
19. Berisha, A. Ab initio exploration of nanocars as potential corrosion inhibitors. *Comput. Theor. Chem.* **2021**, *1201*, 113258. [CrossRef]
20. Kalajahi, S.T.; Mofradnia, S.R.; Yazdian, F.; Rasekh, B.; Neshati, J.; Taghavi, L.; Pourmadadi, M.; Haghirosadat, B.F. Inhibition performances of graphene oxide/silver nanostructure for the microbial corrosion: Molecular dynamic simulation study. *Environ. Sci. Pollut. Res.* **2022**, *29*, 49884–49897. [CrossRef]
21. Benhiba, F.; Hsissou, R.; Abderrahim, K.; Serrar, H.; Rouifi, Z.; Boukhris, S.; Kaichouh, G.; Bellaouchou, A.; Guenbour, A.; Oudda, H. Development of New pyrimidine derivative inhibitor for mild steel corrosion in acid medium. *J. Bio-Tribo-Corros.* **2022**, *8*, 36. [CrossRef]
22. Benhiba, F.; Hsissou, R.; Benzekri, Z.; Echihi, S.; El-Blilak, J.; Boukhris, S.; Bellaouchou, A.; Guenbour, A.; Oudda, H.; Warad, I. DFT/electronic scale, MD simulation and evaluation of 6-methyl-2-(p-tolyl)-1,4-dihydroquinoxaline as a potential corrosion inhibition. *J. Mol. Liq.* **2021**, *335*, 116539. [CrossRef]
23. Deng, S.; Li, X. Inhibition by Ginkgo leaves extract of the corrosion of steel in HCl and H₂SO₄ solutions. *Corros. Sci.* **2012**, *55*, 407–415. [CrossRef]
24. Ngouné, B.; Pengou, M.; Nouteza, A.M.; Nansou-Njiki, C.P.; Ngameni, E. Performances of alkaloid extract from *Rauvolfia macrophylla* Stapf toward corrosion inhibition of C38 steel in acidic media. *ACS Omega* **2019**, *4*, 9081–9091. [CrossRef] [PubMed]
25. Dhoubi, I.; Masmoudi, F.; Bouaziz, M.; Masmoud, M. A study of the anti-corrosive effects of essential oils of rosemary and myrtle for copper corrosion in chloride media. *Arab. J. Chem.* **2021**, *14*, 102961. [CrossRef]

26. Sathiya Priya, A.; Muralidharan, V.; Subramania, A. Development of novel acidizing inhibitors for carbon steel corrosion in 15% boiling hydrochloric acid. *Corrosion* **2008**, *64*, 541–552. [[CrossRef](#)]
27. Zarrouk, A.; Zarrok, H.; Ramli, Y.; Bouachrine, M.; Hammouti, B.; Sahibed-Dine, A.; Bentiss, F. Inhibitive properties, adsorption and theoretical study of 3,7-dimethyl-1-(prop-2-yn-1-yl) quinoxalin-2 (1H)-one as efficient corrosion inhibitor for carbon steel in hydrochloric acid solution. *J. Mol. Liq.* **2016**, *222*, 239–252. [[CrossRef](#)]
28. Pavithra, M.; Venkatesha, T.; Kumar, M.P.; Tondan, H. Inhibition of mild steel corrosion by Rabepazole sulfide. *Corros. Sci.* **2012**, *60*, 104–111. [[CrossRef](#)]
29. Bouklah, M.; Elmsellem, H.; Krim, O.; Serdaroglu, G.; Hammouti, B.; Elidrissi, A.; Kaya, S.; Warad, I. Effect of substitution on corrosion inhibition properties of three Imidazole derivatives on mild steel in 1 M HCl. *Arab. J. Chem. Environ. Res.* **2020**, *7*, 126–143.
30. Bockris, J.M.; Green, M.; Swinkels, D. Adsorption of naphthalene on solid metal electrodes. *J. Electrochem. Soc.* **1964**, *111*, 743. [[CrossRef](#)]
31. Wang, P.; Xiong, L.; He, Z.; Xu, X.; Hu, J.; Chen, Q.; Zhang, R.; Pu, J.; Guo, L. Synergistic Effect of Imidazoline Derivative and Benzimidazole as Corrosion Inhibitors for Q235 Steel: An Electrochemical, XPS, FT-IR and MD Study. *Arab. J. Sci. Eng.* **2022**, *47*, 7123–7134. [[CrossRef](#)]
32. Kowsari, E.; Payami, M.; Amini, R.; Ramezanzadeh, B.; Javanbakht, M. Task-specific ionic liquid as a new green inhibitor of mild steel corrosion. *Appl. Surf. Sci.* **2014**, *289*, 478–486. [[CrossRef](#)]
33. Zehra, B.F.; Said, A.; Eddine, H.M.; Hamid, E.; Najat, H.; Rachid, N.; Toumert, L.I. Crataegus oxyacantha leaves extract for carbon steel protection against corrosion in 1M HCl: Characterization, electrochemical, theoretical research, and surface analysis. *J. Mol. Struct.* **2022**, *1259*, 132737. [[CrossRef](#)]
34. Adewuyi, A.; Oluwaseyifunmi, A.; Kaki, S.S.; Oderinde, R.A. Synthesis of fatty phenylthiosemicarbazide from underutilized *Sesamum indicum* seed oil: A promising corrosion inhibitor of carbon steel in developing country. *SN Appl. Sci.* **2019**, *1*, 637. [[CrossRef](#)]
35. Verma, C.; Obot, I.; Bahadur, I.; Sherif, E.-S.M.; Ebenso, E.E. Choline based ionic liquids as sustainable corrosion inhibitors on mild steel surface in acidic medium: Gravimetric, electrochemical, surface morphology, DFT and Monte Carlo simulation studies. *Appl. Surf. Sci.* **2018**, *457*, 134–149. [[CrossRef](#)]
36. Salman, T.A.; Zinad, D.S.; Jaber, S.H.; Al-Ghezi, M.; Mahal, A.; Takriff, M.S.; Al-Amiery, A.A. Effect of 1,3,4-thiadiazole scaffold on the corrosion inhibition of mild steel in acidic medium: An experimental and computational study. *J. Bio-Tribo-Corros.* **2019**, *5*, 48. [[CrossRef](#)]
37. Zhang, X.; Kang, Q.; Wang, Y. Theoretical study of N-thiazolyl-2-cyanoacetamide derivatives as corrosion inhibitor for aluminum in alkaline environments. *Comput. Theor. Chem.* **2018**, *1131*, 25–32. [[CrossRef](#)]
38. Hu, S.-Q.; Guo, A.-L.; Yan, Y.-G.; Jia, X.-L.; Geng, Y.-F.; Guo, W.-Y. Computer simulation of diffusion of corrosive particle in corrosion inhibitor membrane. *Comput. Theor. Chem.* **2011**, *964*, 176–181. [[CrossRef](#)]
39. Singh, A.; Ansari, K.; Chauhan, D.S.; Quraishi, M.; Lgaz, H.; Chung, I.-M. Comprehensive investigation of steel corrosion inhibition at macro/micro level by ecofriendly green corrosion inhibitor in 15% HCl medium. *J. Colloid Interface Sci.* **2020**, *560*, 225–236. [[CrossRef](#)]
40. Hsissou, R.; Benhiba, F.; Dagdag, O.; El Bouchti, M.; Nouneh, K.; Assouag, M.; Briche, S.; Zarrouk, A.; Elharfi, A. Development and potential performance of prepolymer in corrosion inhibition for carbon steel in 1.0 M HCl: Outlooks from experimental and computational investigations. *J. Colloid Interface Sci.* **2020**, *574*, 43–60. [[CrossRef](#)]
41. Fernine, Y.; Arrousse, N.; Haldhar, R.; Raorane, C.J.; Kim, S.-C.; El Hajjaji, F.; Touhami, M.E.; Beniken, M.; Haboubi, K.; Taleb, M. Synthesis and characterization of phenolphthalein derivatives, detailed theoretical DFT computation/molecular simulation, and prevention of AA2024-T3 corrosion in medium 3.5% NaCl. *J. Taiwan Inst. Chem. Eng.* **2022**, *140*, 104556. [[CrossRef](#)]

Disclaimer/Publisher's Note: The statements, opinions and data contained in all publications are solely those of the individual author(s) and contributor(s) and not of MDPI and/or the editor(s). MDPI and/or the editor(s) disclaim responsibility for any injury to people or property resulting from any ideas, methods, instructions or products referred to in the content.